Heliyon 10 (2024) e26398

Contents lists available at ScienceDirect

Heliyon

journal homepage: www.cell.com/heliyon

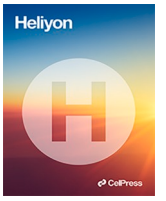

Research article

Design and performance analysis of an L-shaped radiator and defected ground antenna for enhancing wireless connectivity in brain implants

Anupma Gupta [a], Vipan Kumar [b], Mohammed H. Alsharif [c], Peerapong Uthansakul [d,*], Monthippa Uthansakul [d], Vigneswaran Dhasarathan [e], Manish Sharma [f]

[a] *Department of Interdisciplinary Courses in Engineering, Chitkara University Institute of Engineering and Technology, Chitkara University, Punjab, India*
[b] *Department of ECE, Sri Sai College of Engineering and Technology, Badhani, Pathankot, India*
[c] *Department of Electrical Engineering, College of Electronics and Information Engineering, Sejong University, Seoul, 05006, Republic of Korea*
[d] *School of Telecommunication Engineering, Suranaree University of Technology, Nakhon Ratchasima, 30000, Thailand*
[e] *Department of Electronics and Communication Engineering, Centre for IoT and AI (CITI), KPR Institute of Engineering and Technology, Coimbatore, 641407, India*
[f] *Chitkara University Institute of Engineering & Technology, Chitkara University, Punjab, 140401, India*

ARTICLE INFO

Keywords:
L-shaped defected ground
BID
Implantable antenna
Specific absorption rate

ABSTRACT

Brain implantable wireless microsystems has potential to treat neurological diseases and maintain the quality of life. Highly efficient miniaturized antenna is the fundamental part of BID (brain implantable device) for reliable signaling of data through dissipative intracranial material. In this paper, a patch antenna with L-shaped defected ground is demonstrated. L-shaped radiator contributed to achieve the resonance at 2.45 GHz industrial scientific and medical (ISM) band. Antenna size is reduced to $10 \times 10 \times 0.25$ mm^3. The proposed L-shaped ground plane geometry is contributing in improving the radiation performance. |S11| value shifts from 15 dB to 30 dB after modifying the ground plane. Proposed structure attained the gain of −14 dBi when located between the Dura and CSF layers at the depth of 12 mm in human brain model. Full wave simulated antenna prototype is fabricated and measured for performance verification. Impedance bandwidth of 270 MHz and broadside radiation pattern (for transferring maximum electromagnetic energy away from tissue) are maintained by the proposed antenna. Brain tissue safety is ensured by specific absorption rate which is 0.709 W/kg and in compliance with the safety limits of 1.6 W/kg for 1-g averaged tissue. Proposed antenna structure is the promising candidate for medical implant technology.

1. Introduction

Wireless communication is playing important role in people's lives and becoming impossible to sustain lacking it. Among the

* Corresponding author.
E-mail addresses: anupmagupta31@gmail.com (A. Gupta), er.vipingupta14@gmail.com (V. Kumar), uthansakul@sut.ac.th (P. Uthansakul), mtp@sut.ac.th (M. Uthansakul), manish.sharma@chitkara.edu.in (M. Sharma).

https://doi.org/10.1016/j.heliyon.2024.e26398
Received 7 September 2023; Received in revised form 6 February 2024; Accepted 12 February 2024
Available online 16 February 2024

different applications of the telecommunication, wireless bio-telemetry is evolving rapidly for the benefits of patients and doctors. It deals with the transmission of vital physiological parameters for diagnosis of tailored diseases, treatment and real-time monitoring. Brain Implantable Devices (BIDs) have gained wide expansion in the field of wireless bio-telemetry. BIDs help the patients suffering with neurological disorders for the early detection and diagnosis of epileptic seizures, restoring of lost sensory information and functionalities of paralyzed individuals, in brain-machine-interfaces for decoding of neurons, and neurological therapies. BID consists of various components, including sensor, signal processing unit, a program for simulating the brain, a communication link to interact with an external unit [1–3]. Reliable BMI systems are currently being created. Systems for recording neural activity must be extremely small, biocompatible, wirelessly powered, and capable of data transmission in reliable way. The task of removing the brain signal data from the implanted equipment is the most challenging and promising one [4,5]. Brain implantable medical devices hardly use wired system to link with external units as it can impend the care of the patients and bounds their body movements [6,7]. Thus, more consideration has now turned for the wireless link. Fig. 1 shows the schematic view of the wireless brain monitoring system. Implantable antenna integrated with a neural sensor module is implanted in the head.

Neural signals like variation of tissue effective permittivity, temperature, CSF pressure are transmitted through the broadside radiation pattern of implanted antenna to the external receiver antenna for data processing. Antenna is the crucial part of the reliable wireless bio-telemetry system. The antenna for such a system is quite difficult to design.

The complex structure of human brain which consists of heterogeneous layers of varying permittivity, conductivity, and thickness; it hinders the propagation of electromagnetic radiations [8]. Thus, brain implantable antenna designing has its own difficulties like impedance matching, frequency detuning, broadside radiation pattern, miniaturization, and ensuring the safety of brain from near-field reactive power [9]. Different techniques are adopted by the engineers to enhance different features of antenna [10–15].

Brain implantable antenna needs to fit in the extremely small area of the integrated circuit, thus various antenna miniaturization techniques are proposed by researchers. Spiral and meandered radiator [16,17] with offset fed [18], defected ground using open end slots [19–21], shorting pin [22], inductive and capacitive coupling [23,24] are the commonly used techniques for antenna size reduction. However, gain and radiation characteristics of these antennas is reduced with size reduction. To overcome the antenna frequency detuning and impedance mismatch effect, wide bandwidth and multi-band configurations are suggested in Refs. [25–28]. Furthermore, to make antenna biocompatible, antenna is coated with high dielectric low loss materials [29,30], insulated with deionized water to escape the direct contact of antenna with brain [31]. Different gain enhancement approaches like end fire structures [32], PIFA [33] and LC tank circuit based technologies [34] are used in the recent literature. Most of the structures possesses larger and complex geometry. Larger area limits the usage of antenna in BMDs, shorting pins and multiple slotting requires very vigilant alignment during the fabrication of such compact antennas. Compact and planar antenna structures with higher gain, and broader bandwidth are preferred for brain implantable devices. Free space literature shows that patch antenna radiation performance can be improved effectively by incorporating defected ground technology [35,36]. Besides this, performance of most of the present antennas are analyzed in the homogeneous brain phantom at low depth of about 5 mm whereas brain is a complex multi-layered heterogeneous

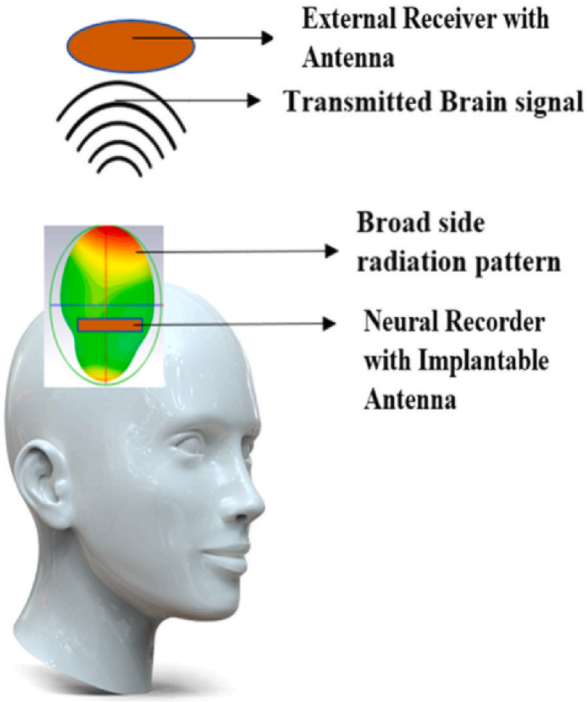

Fig. 1. Schematic view of the implantable antenna's role in wireless brain monitoring system.

Table 1
Comparison of the current contribution with the previous related works.

Ref.	Frequency GHz	Volume (mm^3)	Impedance bandwidth (MHz)	Gain (dBi)	SAR (W/kg) 1-g tissue	Substrate Material	Design Technology
[18]	2.45	39.3	330	−27.2	568.2 with 2.8 mW	Rogers 3210	Circular slotted patch
[20]	2.45	98	450	−16	0.494 with 1 mW	Rogers 3010	Meandered patch
[5]	915, 2450	8 × 6 × 0.5	90,210	−28.5, −22.5	971.56, 807.34 with 1W	Rogers 6010	Meandered stack patch
[22]	2.45	9.8	1038.7	−20.71	289.76 for 1 W	Ultralam (liquid crystal polymer)	Meandered patch with shorting pins
[24]	2.45	127	260	−20.4	213 with 7.51 mW	Rogers 3010	Multiple meandered slots and slits
[37]	3.1–11.5	30 × 25 × 0.8	8.4 GHz	4.8 dB (on body)	1.23	RT Duroid 5880	Ashoka chakra shaped radiator with CPW feed for on body wearable applications
[38]	2.5	58 × 40 × 0.8	650 MHz	−26.2 dBi	0.469 with 300 mW	Polyimide, FR4	Parasitic loaded antenna with DGS
This work	**2.45**	**25**	**270**	**−14.57**	**0.709 with 1 mW**	**RO 3010**	**Defected ground with L-shaped radiator**

structure. Table 1 presents a comparison between the current contribution and previous works in the field. This antenna has minimum volume except in Ref. [22] with maximum gain and simple geometry. Most of the implantable antenna are designed using the complex meandered line structure, shorting pins and stacked patch geometries. The proposed structure has simple configurations with better radiation performance. It makes antenna suitable to integrate with integrated circuits and reduces fabrication complexities. Rogers 3010 material contributes to increases fringing effect and reduces resonance current length, and have low tangent losses of 0.0009 as compared to FR4.

Therefore, in this paper, authors have proposed an antenna with higher gain and compact size that can be implanted deep inside the brain at the depth of 12 mm. CST microwave studio is used to design the antenna and a seven-layer brain phantom. Thin layer of high dielectric material Ro 3010 is used to insulate the antenna conducting part from brain tissue to avoid the impedance distortion.

- Miniaturized to 0.08 $\lambda_o \times 0.08\ \lambda_o$, where λ_o is free space wavelength at 2.45 GHz.
- Wider bandwidth to withstand frequency detuning effect with improved impedance matching.
- Higher gain of −14 dBi with broadisde radiation pattern.
- Low SAR value of 0.709 W/kg for 1 mW input power, making antenna safe to transfer low power electromagnetic signal through bio tissues.

Section 2 describes the properties of brain tissue used for simulaion model, and antenna configuration. In section3 antenna behavior is assessed in terms of |S11|, bandwidth, gain and radiated power patterns. Finally, in section brain tissue safety is ensured from the electromagnetic radiations by evaluating the SAR value.

2. Brain tissue modeling and antenna configurations

Characterization of antenna with the accurate brain model is quite hard. Thus, a simplified munerial model consists of seven different layers is used for the simulation setup. Size of this phantom model is 85 mm × 85 mm × 72.2 mm. Size of the brain model is sufficciently large to avoid the diffraction of EM waves from edges. Thickness and electrical properties of different layers are taken from the data mentioned in Refs. [8,21–23] and listed in Table 2.

In Fig. 2(a) simulation model is shown with the implanted antenna between CSF and Dura layers of brain. Implantable devices are deployed mostly above the cerebral spinal fluid (CSF) which act as a protective layer for spine and cortex and reflects the physiological and pathological changes occurring in the brain [24]. Each body organ has different tissue layers and implantable devices are need to be deployed in between the different tissue layers. Thus, antenna is also implanted in the single layer muscle phantom of size 80 mm × 80 mm × 15 mm at a depth of 5 mm (in Fig. 2(b)) and a voxel arm shoulder at a depth of 2 mm (in Fig. 2(c)) for reliability of antenna performance when deployed in different tissue layer in real time applications. Different implant depths are considered for different implant locations as skin implant (2 mm), CSF implant (12 mm), scalp implant (4 mm) [5,18,22,24,39]. Therefore, the proposed is also deployed at different depth of different tissues.

Topology of the proposed structure is represented in Fig. 3. A defected ground patch antenna structure is designed on dielectric material of RO 5880 with depth of 0.125 mm, ε_r (relative permittivity) value of 2.2 and δ (loss tan) value of 0.0009. In defected ground technology ground plane is modified to enhance the antenna performance. Planar size of the structure is 10 mm × 10 mm which is eqvivalent to 0.08 λo × 0.08 λo, where λo represents the free space wavelength at 2.4 GHz. An L-shaped radiator and L-shaped defected ground is designed to attain impedance matching and tuning the antenna at 2.45 GHz.

Conducting part is isolated from brain tissue layers by adding two layers of the dielectric material RO3010 above the radiator and below the ground plane with depth of 0.125 mm, ε_r (relative permittivity) value of 10.2 and δ (loss tan) value of 0.0022. Surface current plot in Fig. 3 represents the current path trace by antenna at 2.45 GHz. It is clear that antenna has followed a single resonance current path for the operating frequencies. It helps to mitigate the effect of harmonic frequencies and makes antenna more resist to interference of other frequencies.

To facilitate a better understanding of how to determine the structure of antennas for biological tissue implantation, equivalent dielectric constant is calculated. Equivalent dielectric value is incorporated with the fundamental free space formulas. Following design equations are considered to design the patch antenna.

For the 2.45 GHz resonance frequency (f_0) at quarter wavelength, with equivalent dielectric (ε_{eqv}) value in multiple brain tissue layer and height (h) of antenna, width (w) of patch is calculated by Equation (1). Here, the physical dimensions of antenna are considered according to the quarter wavelength to design a compact structure for implantable devices. Effective resonance path of half

Table 2
Brain tissue properties at 2.45 GHz [8,21].

Tissue Layer	Thickness (mm)	Loss tangent	Dielectric constant
CSF	2	0.385	66.319
White Matter	3.7	0.271	48.994
Gray Matter	55	0.246	36.226
Dura	1.5	0.292	42.099
Skin	1.0	0.273	42.923
Fat	2	0.145	5.285
Cortical Bone	7	0.252	11.410

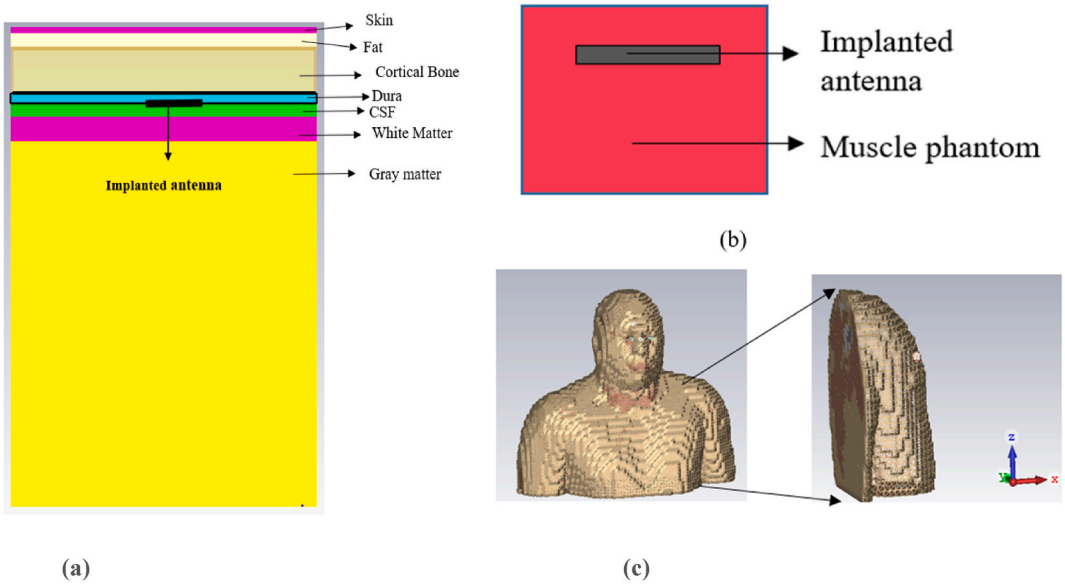

Fig. 2. Simulation setup showing the position of implanted anetnna (a) inside the seven layer brain tissue, (b) homogeneous muscle phantom and (c) voxel shoulder.

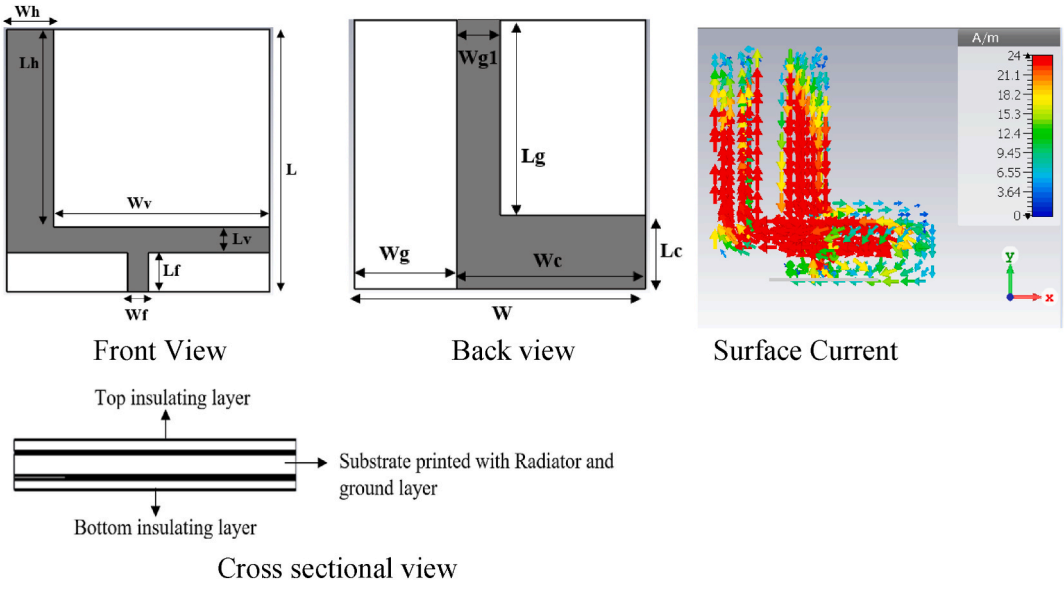

Fig. 3. Geometry of the designed antenna and surface current distribution at 2.45 GHz.

wavelength is created by modifying the patch shape. To make antenna resonate, half wavelength dimensions is required (according to equation (3)).

$$w = \frac{c}{4f_0\sqrt{\frac{\varepsilon_{eqv}+1}{2}}} \tag{1}$$

Length of antenna (l) is patch is calculated by Equations (2) and (3). c is the speed of light and ε_{reff} is the effective dielectric constant due to fringing effect of antenna.

$$\varepsilon_{reff} = \frac{\varepsilon_{eqv}+1}{2} + \frac{\varepsilon_{eqv}-1}{2}\left[1+12\frac{h}{w}\right]^{-0.5} \tag{2}$$

$$l = \frac{c}{2f_0\sqrt{\varepsilon_{reff}}} - 0.824h\left(\frac{\left(\varepsilon_{reff}+0.3\right)\left(\frac{w}{h}+0.264\right)}{\left(\varepsilon_{reff}-0.258\right)\left(\frac{w}{h}+0.8\right)}\right) \tag{3}$$

As antenna is implanted in brain tissue which is a complex and lossy multilayered structure with heterogeneous electric properties. Thus, dialectic constant of antenna needs to be evaluated as multiple dielectric layers. Krasweski model for equivalent substrate model of multilayer structure is considered here in Equation (4) [39,40]. Here, a method to determine the effective permittivity of a substrate with two layers is presented. Same methodology is followed for all brain layers to determine a single substrate layer with an equivalent permittivity (ε_{eqv}). The equivalent substrate model designed from Krasweski model is shown in Fig. 4 (a and b).

$$\varepsilon_{eqv} = \left[\sqrt{\varepsilon_{r2}} + vi\left(\sqrt{\varepsilon_{r2}} - \sqrt{\varepsilon_{r1}}\right)\right]^2 \tag{4}$$

Where *vi* is the surface volume of the layer i and calculated by dividing the volume of the layer i over the total volume. ε_{ri} gives the relative permittivity of the layer i.

Now, based on the antenna geometry, effective resonating current length (LR) of the antenna can be calculated through the surface current distribution in Fig. 3. The current length Equation form antenna geometry is calculated through Equation (5).

$$LR = Wv + Lh + Wh \tag{5}$$

Where, Wv, Wh and Lh are the dimensions of antenna and given in Table 3. According to antenna theory, resonance frequency is related to radiating path length as given in Equation (6).

$$LR = \frac{c}{2f_r\sqrt{\varepsilon_{reff}}} \tag{6}$$

The value of ε_{reff} is 12.345 which is calculated through Equations (2) and (4). At 2.45 GHz, required half wave resonance length is approximately 17.44 mm. It shows that the calculated radiating path length from the antenna design topology is in good agreement with the numerically simulated value. Further, to explain the behavior of designed topology antenna-design process is described in 3-steps which are represented in Fig. 5. Input reflection-coefficient plot of 3-design steps is explained in Fig. 6.

Step1: Initially, a full ground plane antenna with L-shaped radiator is designed and tuned at 4 GHz in the brain phantom (Fig. 5(a and b)). Width 'wh' of the vertical-arm of L-shaped-radiator has substantial effect on impedance-matching and setting up the resonance frequency for this electrically small antenna. Reflection-coefficient for the parametric-analysis of 'wh' is characterized in Fig. 7. Value of 'wh' is changed from 0.5 mm to 4.5 mm. Reducing width of radiator origins leftward-shifting of resonance but after 'wh = 1.5 mm' impedance matching starts reducing (reflection coefficient value increases). Thus, width 'wh' of vertical arm of radiator is consider as 1.5 mm for further design process. Then, antenna is successively modified to resonate at 2.45 GHz by defected ground structure.

Step2. Surface current of antenna is observed to analyze antenna operation and represented in Fig. 8(a). It can be found that surface current on ground plane is concentrated towards the edge which is below the radiator. Coupling between ground plane and radiator is modified by shifting the ground plane edge towards the inner side of radiator arm (Fig. 5(c)). It causes significant impact of lowering the antenna resonance frequency at desired value of 2.45 GHz (at quarter wavelength). Ground plane edge is shifted by the dimension 'wg' and its value is found through the parametric analysis. Value of wg is changed from 4.2 mm to 0.5 mm and its effect on resonance frequency is shown by reflection coefficient plots in Fig. 9. With increasing value of 'wg', resonance frequency is reducing. Rate of frequency reduction is also decreasing with lower values of 'wg'. Desire resonance frequency for ISM band is obtained at 3.2 mm with reflection coefficient of −16 dB.

Step3: Furthermore, in step3, ground-plane is further reformed to improve the impedance-matching. Present literature shows that antenna impedance may diminishes when implanted at different depth and different body. Thus, to enhance the reliability of proposed structure for practical application, reflection coefficient is improved by modifying the ground plane as L-shaped (Fig. 5(d)). Surface current of step2 (Fig. 8(b)) shows that no surface current is flowing toward the right side of the ground. Therefore, portion of null current on ground plane is etched. Length of the etched part is changed to gain maximum reflection-coefficient at 2.45 GHz. Fig. 10 shows the parametric analysis of reflection coefficient for the vertical arm length ('Lc') of ground plane. As the width is reduced, reflection coefficient plot shifts downward without altering the resonance frequency. Optimum results are achieved at Lc = 2.125 mm. On reducing more, it causes detuning of the resonance frequency. Then, all the parameters of the proposed-structure optimized together and summarized in Table 3.

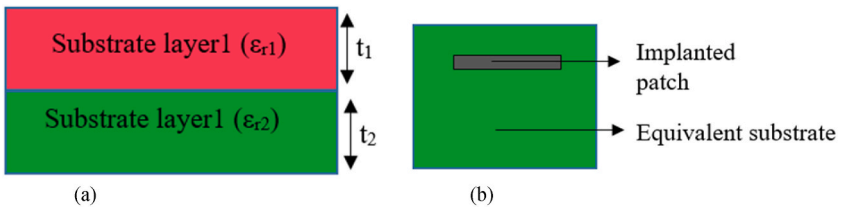

Fig. 4(a). Krasweski model and (b) Equivalent single dielectric layer.

Table 3
Geometrical parameters of the designed antenna.

Parameter	Value (mm)	Parameter	Value (mm)
W	10	L	10
Wf	0.8	Lf	1.5
Wv	8.5	Lv	0.95
Wg1	2.37	Wc	6.8
Wg	3.2	Lc	2.125
Lg	7.875	Lh	7.55
Wh	1.5		

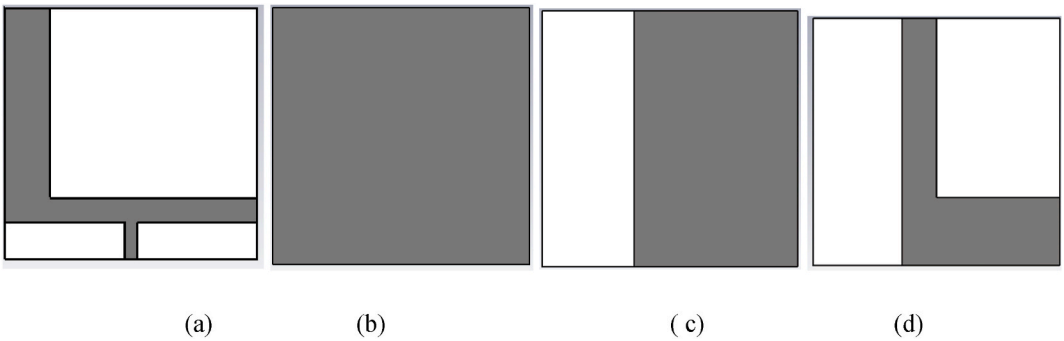

Fig. 5. (a) Step wise design evaluation of antenna (a) radiator for all steps (b) step1 ground plane (c) step2 ground plane and (d) step4 ground plane (proposed).

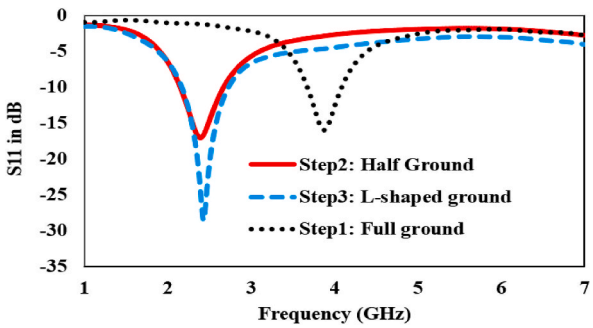

Fig. 6. Step wise Reflection coefficient of the designed antenna.

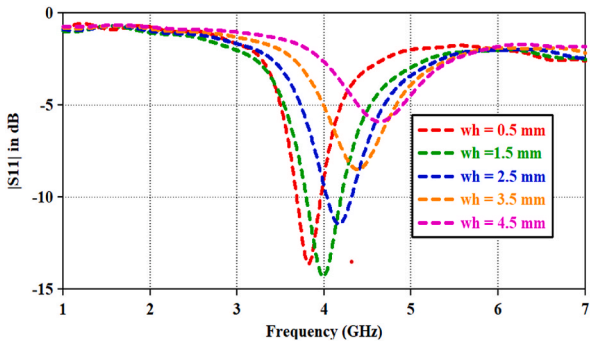

Fig. 7. Reflection coefficient plot for varying 'wh'.

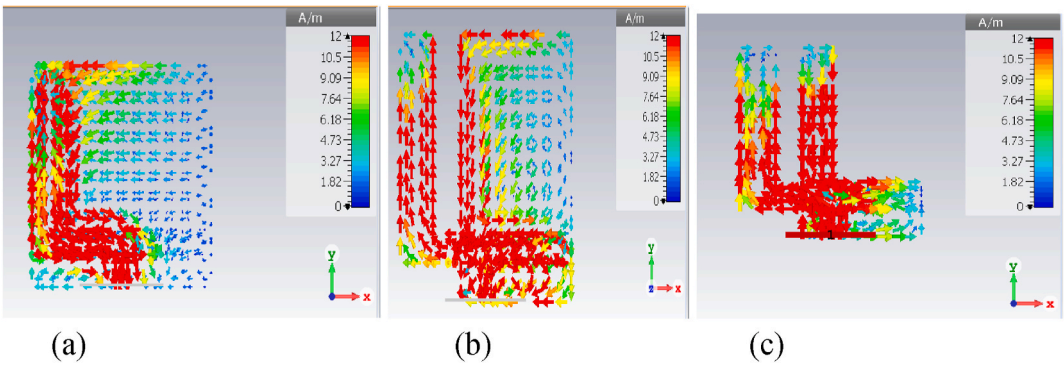

Fig. 8. Stepwise surface current (a) step1 (b) step2 (c) Step3.

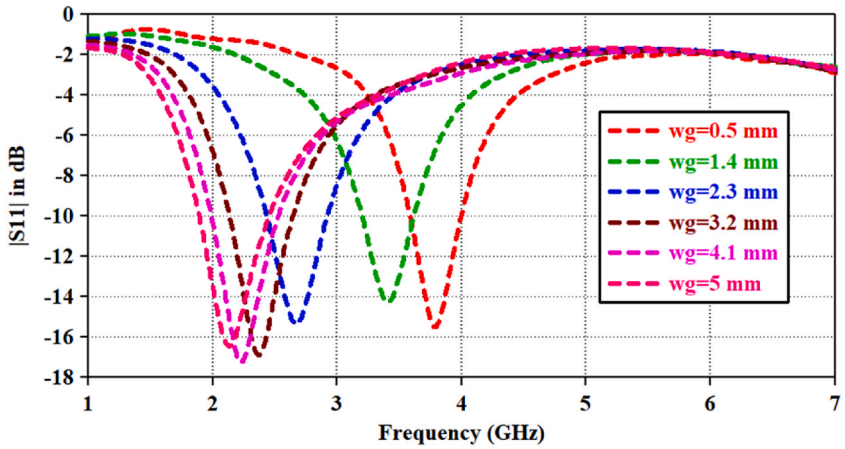

Fig. 9. Reflection coefficient plot for varying 'wg'.

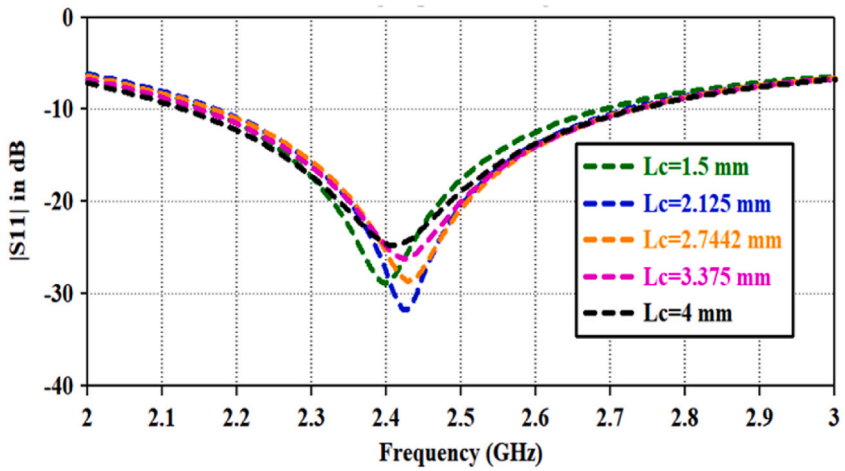

Fig. 10. Reflection coefficient plot for varying 'Lc'.

Moreover, modifying the ground plane in step3 has shown significance impact on radiation characteristics. Radiation efficiency plot for the step2 and step3 is shown in Fig. 11. Radiation efficiency is increased by 3% in the L-shaped ground. Radiation efficiency of 7.2 % is attained in step3 and 4.4 % in step2. To justify this, 3-D and 2-D directivity plots are shown in Fig. 12. It shows that in step2 radiations are oriented towards the parallel to the surface of tissues (in Fig. 12 (a and b)) whereas in the step3 radiations are oriented towards the normal of surface of tissues (in Fig. 12 (c and d)). It is the most desired feature of implantable antenna to establish the

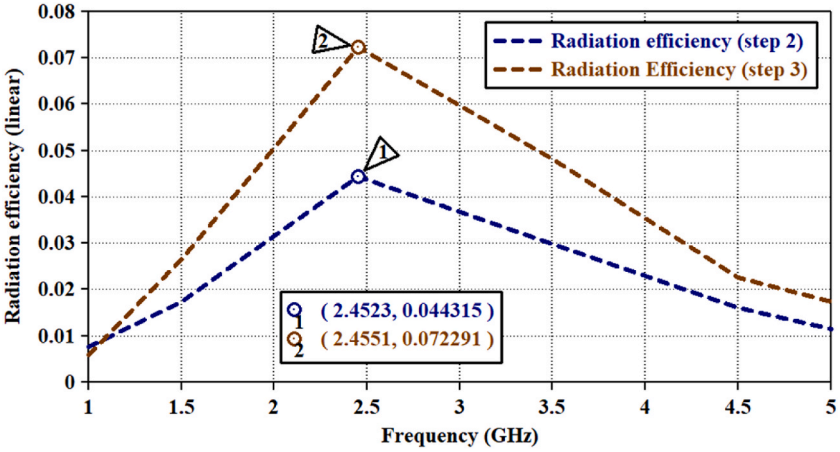

Fig. 11. Plot for Radiation efficiency.

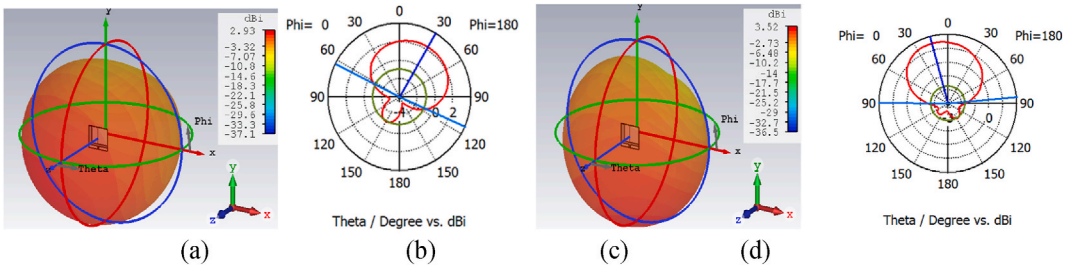

Fig. 12. Directivity plot (a and b) step2 (c and d) for step3.

reliable communication link. L-shaped ground plane in step3 (Fig. 8(c)) has surface current concentration on the vertical arm of the ground plane that causes the orientation of radiations towards the +z direction (away from the head). Directivity of antenna in step2 is 2.93 dBi and increased to 3.52 dBi in step3.

Low efficiency in implantable antenna is due to power absorbed by the brain tissues. Present antenna has higher efficiency than some of the reported literature as 5% in Ref. [11], 1% in Ref. [23], and 6.5% in Ref. [20]. Fig. 6 depicts that bandwidth is constant for both the step2 and step3. It is due to the single resonance current path of antenna in both the structures. Surface current reveals that no other resonance path is excited when ground plane is modified. Wider bandwidth occurs due to the merging of multiple resonance path [41,42].

Very low amount of power is lost by antenna structure, impedance mismatch and surface waves. Power loss characteristics for the antenna are shown in Fig. 13 and listed in Table 4. Antenna is simulated for 0.5W of input power. Maximum power is lost in the dura and CSF layer of the brain where antenna is implanted. It is clear that antenna impedance mismatch loss at port and substrate material

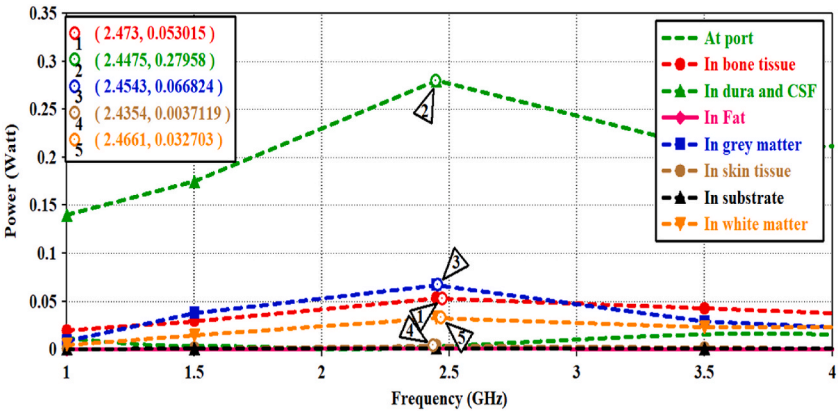

Fig. 13. Plot for power lost in brain tissue layers.

Table 4
Value of power loss at 2.45 GHz in brain.

Layers	Power loss (Watt)	Layers	Power loss (Watt)
Skin	0.00374	White Matter	0.03284
Fat	0.00113	Gray Matter	0.06693
Bone	0.05323	Dielectric	0.00118
Dura and CSF	0.2797	Total loss	0.4418
At port (impedance mismatch)	0.003167		

loss are negligible small.

3. Results and discussions

Simulated results are validated by measuring the antenna performance of the fabricated prototype (in Fig. 14 (a and b). Antenna is inserted in the animal tissue for implant application (in Fig. 14 (c and d)). Shape of the animal tissue is not symmetrical, normalized dimensions of the tissue is $30 \times 40 \times 10$ mm^3. Pictures of the measurement-setup are presented in Fig. 14.

In Fig. 15, comparison of the measured reflection coefficient with simulated is represented. Both the results are in good agreement with each other for required resonance frequency band. Simulated |S11| plot shows the 10-dB impedance-bandwidth of 490 MHz (ranging from 2.19 GHz to 2.68 GHz). Measured graph represents the bandwidth of 270 MHz (2.32GHz–2.59 GHz). It shows that simulated bandwidth is broader than measured bandwidth. It is possibly due to difference between the phantom structure used for numerical simulation and measurement setup. Highly lossy multilayer structure tends to reduce the quality factor of antenna which increases the bandwidth (BW = fr/Q). Similar difference in simulation and measurement set up is also witnessed in Refs. [22,27]. Antenna simulated reflection plot for homogeneous tissue phantom is also represented which justify the antenna measured results in pork tissue. Antenna is deployed in the voxel shoulder phantom at the depth of 2 mm, reflection plot sows that resonance bandwidth is constant with slight upward shifting of curve. It ensures the robustness of antenna for heterogeneous tissue environment for different human beings.

Radiation-plots at 2.45 GHz are displayed in Fig. 16, showing forward-directed-beam in both the E-plane and H-plane orientations. In E-plane broadside radiation pattern is achieved with maximum simulated gain of −14.27 dB and measured gain of −14.57 dB oriented towards the external monitoring device. In H-plane unidirectional radiation pattern is attained for both simulated and measured environment. Null is occurring at 255° (towards the normal to the surface of body), and gain of −12.57 dB and −13.87 dB is found for simulated and measured data. This type of radiation characteristics is the required feature for an antenna to be used in the implantable devices.

Patient safety is the major concern for implantable antenna design. Some of the radiating EM power is absorbed by the brain tissues, which is risky if go beyond some levels. SAR is the safety parameter to monitor the level of radiation absorption by body tissue. IEEE Std C95.1–1999 complying the SAR limit to 1.6 W/kg over 1- gram of tissue. Numerical simulation for SAR analysis is performed with the seven-layered brain phantom with input power of 10 mW over 1-g of tissue. Fig. 17 shows the simulated results and confirms the safety of proposed antenna for implant application. SAR of designed antenna is 0.709 W/kg for brain phantom (in Fig. 17 (a and b)) and 0.987 W/kg for voxel shoulder phantom (in Fig. 17 (c)). Thus, allowable input power for this structure is much higher than IEEE safety regulation (25 μW).

Fig. 14. Photographs during measurement (a) antenna without superstrate (b) with superstrate (c) antenna in animal tissue (d) antenna in anechoic chamber.

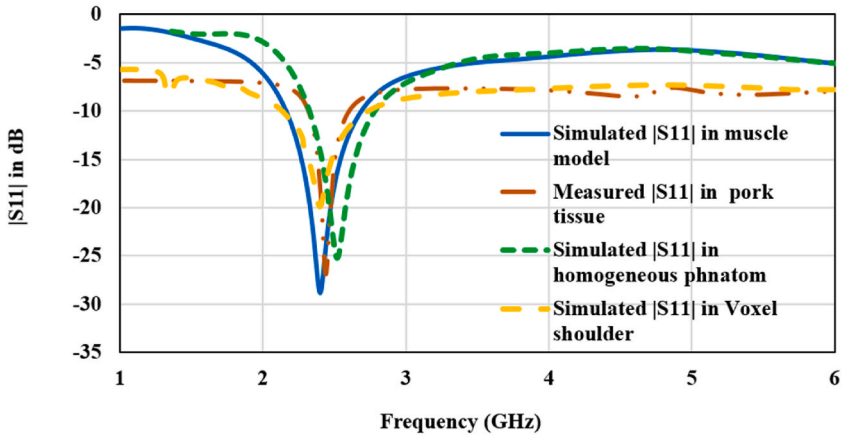

Fig. 15. Reflection coefficient plot for measured and simulated results.

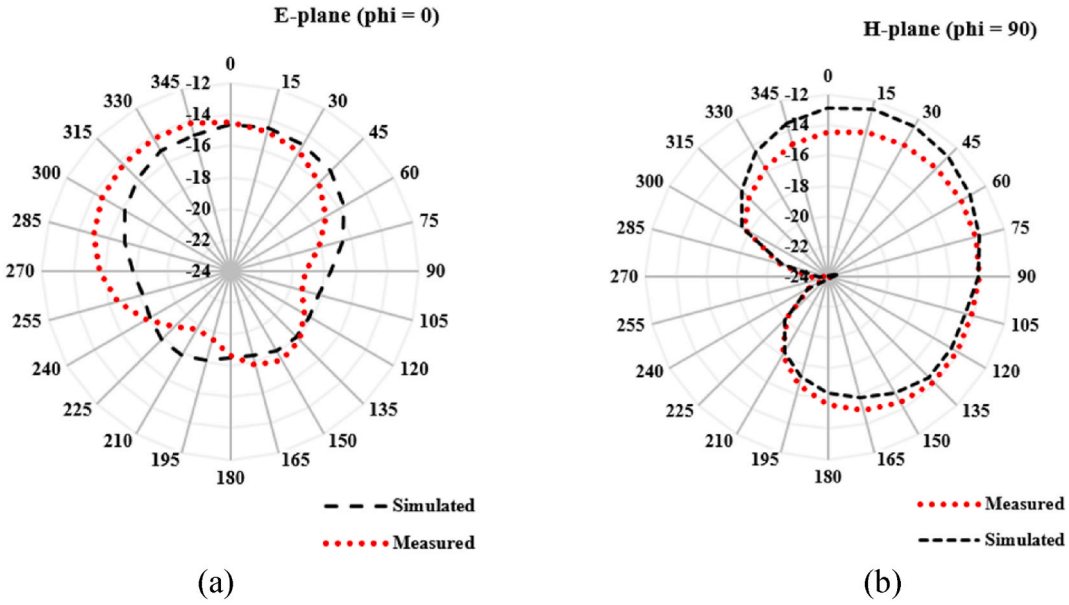

Fig. 16. Radiation pattern at 2.45 GHz in (a) E-plane and (b) H-plane.

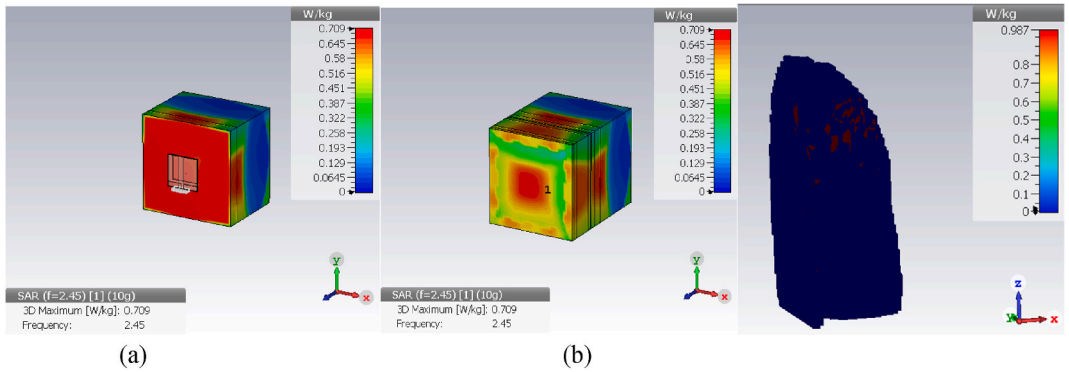

Fig. 17. SAR of the proposed structure (a) top layers hidden (b) top layers shown (c) in voxel shoulder.

4. Conclusions

A miniaturized brain implantable antenna is designed and numerically simulated while embedded in the seven-layer brain phantom. Antenna has footprint of 10×10 mm^2 because of the L-shaped radiator and ground. Identical parallel radiator and ground not only promoted miniaturization but also improved gain and bandwidth. Topology of antenna structure is optimized to operate at 2.45 GHz frequency. A prototype is fabricated to measure the antenna performance. Pork tissue is used to embed the fabricated antenna while measurement. Overlapping simulated and measured bandwidth is 270 MHz which is broad enough to withstand the frequency detuning effect caused by the frequency dependent heterogeneous electrical properties of brain. Proposed structure exhibited wider bandwidth and high gain; both parameters are critical for transmission of neurological signal. Broadside radiation pattern with −14.57 dBi gain in E-plane and −13.87 dBi in H-plane is achieved which is higher than the other implantable antennas presented in current literature. SAR value is 0.709 W/kg making antenna safe for brain tissue.

Funding

"This work was supported by (i) Suranaree University of Technology (SUT), (ii) Thailand Science Research and Innovation (TSRI) and (iii) National Science, Research and Innovation Fund (NSRF)".

CRediT authorship contribution statement

Anupma Gupta: Writing – original draft, Validation, Methodology, Conceptualization. **Vipan Kumar:** Methodology, Investigation, Data curation, Conceptualization. **Mohammed H. Alsharif:** Writing – original draft, Validation, Project administration, Formal analysis. **Peerapong Uthansakul:** Writing – review & editing, Validation, Supervision, Resources, Funding acquisition. **Monthippa Uthansakul:** Writing – review & editing, Validation, Investigation. **Vigneswaran Dhasarathan:** Writing – review & editing, Visualization, Validation. **Manish Sharma:** Writing – review & editing, Visualization, Validation.

Declaration of competing interest

The authors declare that they have no known competing financial interests or personal relationships that could have appeared to influence the work reported in this paper.

References

[1] J. Andreu-Perez, D.R. Leff, H.M.D. Ip, G. Yang, From wearable sensors to smart implants–toward pervasive and personalized healthcare, IEEE (Inst. Electr. Electron. Eng.) Trans. Biomed. Eng. 62 (12) (2015).
[2] I. Ahmad, H. Dildar, W. Khan, S. Shah, S. Ullah, S. Ullah, S. Umar, M.A. Albreem, M.H. Alsharif, K. Vasudevan, Design and experimental analysis of multiband compound reconfigurable 5G antenna for sub-6 GHz wireless applications, Wireless Commun. Mobile Comput. 2021 (2021).
[3] M.H. Alsharif, Comparative analysis of solar-powered base stations for green mobile networks, Energies 10 (2017) 1208.
[4] B. Rana, et al., An implantable antenna with broadside radiation for a brain machine interface, IEEE Sensor. J. 19 (20) (2019) 9200–9205.
[5] S.A.A. Shah, H. Yoo, Scalp-implantable antenna systems for intracranial pressure monitoring, IEEE Trans. Antenn. Propag. 66 (4) (2018) 2170–2173.
[6] G. Kumar, R. Kumar, A survey on planar ultra-wideband antennas with band notch characteristics: principle, design, and applications, AEU-International Journal of Electronics and Communications 109 (2019) 76–98.
[7] M. H Alsharif, M. Hossain, A. Jahid, M. Khan, B.J. Choi, S. M Mostafa, Milestones of wireless communication networks and technology prospect of next generation (6G), Comput. Mater. Continua (CMC) 71 (2022) 4804–4818.
[8] S.M. Asif, A. Iftikhar, B.D. Braaten, D.L. Ewert, K. Maile, A wide-band tissue numerical model for deeply implantable antennas for RF-powered leadless pacemakers, IEEE Access 7 (2019) 31031–31042.
[9] A. Sharma, E. Kampianakis, M.S. Reynolds, A dual-band HF and UHF antenna system for implanted neural recording and stimulation devices, IEEE Antenn. Wireless Propag. Lett. 16 (2017) 493–496.
[10] B. Lee, et al., An implantable peripheral nerve recording and stimulation system for experiments on freely moving animal subjects, Sci. Rep. 8 (1) (Dec. 2018) 1–12.
[11] M.H. Alsharif, Y.H. Alsharif, S. Chaudhry, M.A. Albreem, A. Jahid, E. Hwang, Artificial intelligence technology for diagnosing COVID-19 cases: a review of substantial issues, Eur. Rev. Med. Pharmacol. Sci. 24 (2020) 9226–9233.
[12] M. H Alsharif, A. Jahid, R. Kannadasan, M.-K. Kim, Unleashing the potential of sixth generation (6G) wireless networks in smart energy grid management: a comprehensive review, Energy Rep. 11 (2024) 1376–1398.
[13] D. Nikolayev, M. Zhadobov, R. Sauleau, Immune-to-detuning wireless in-body platform for versatile biotelemetry applications, IEEE Trans. Biomed. Circuits Syst. 13 (2) (Apr. 2019) 403–412.
[14] Y. Liu, Y. Chen, H. Lin, F.H. Juwono, A novel differentially fed compact dual-band implantable antenna for biotelemetry applications, IEEE Antenn. Wireless Propag. Lett. 15 (2016) 1791–1794.
[15] Z.-J. Yang, L. Zhu, S. Xiao, An implantable wideband microstrip patch antenna based on high-loss property of human tissue, IEEE Access 8 (2020), 93048–930572020.
[16] S. Xiao, C. Liu, Y. Li, X.M. Yang, X. Liu, Small-size dual-antenna implantable system for biotelemetry devices, IEEE Antenn. Wireless Propag. Lett. 15 (2016) 1723–1726.
[17] I.A. Shah, M. Zada, H. Yoo, Design and analysis of a compact sized multiband spiral-shaped implantable antenna for scalp implantable and leadless pacemaker systems, IEEE Trans. Antenn. Propag. 67 (6) (Jun. 2019) 4230–4234.
[18] Samnang Hout, Jae-Young Chung, Design and characterization of a miniaturized implantable antenna in a seven-layer brain phantom, IEEE Access 7 (2019) 162062–162069.
[19] F. Faisal, M. Zada, A. Ejaz, Y. Amin, S. Ullah, H. Yoo, A miniaturized dual-band implantable antenna system for medical applications, IEEE Trans. Antenn. Propag. 68 (2) (Feb. 2020) 1161–1165.
[20] V.K. Gupta, P. Mehra, Design and analysis of brain-implantable antenna for neural signal transmission, in: S. Mekhilef, M. Favorskaya, R.K. Pandey, R.N. Shaw (Eds.), Innovations in Electrical and Electronic Engineering, Lecture Notes in Electrical Engineering, vol. 756, Springer, Singapore, 2021, https://doi.org/10.1007/978-981-16-0749-3_37.

[21] L. Luo, B. Hu, J. Wu, T. Yan, L.-J. Xu, Compact dual band antenna with slotted ground for implantable applications, Microw. Opt. Technol. Lett. 61 (2019) 1314–1319.
[22] Naeem Abbas, Ali Shah Syed Ahson, Abdul Basir, Zubair Bashir, Adeel Akram, Hyoungsuk Yoo, Miniaturized antenna for high data rate implantable brain-machine interfaces, IEEE Access 10 (2022) 66018–66027.
[23] Shubin Ma, Toni Björninen, Lauri Sydänheimo, Merja H. Voutilainen, Leena Ukkonen, Double split rings as extremely small and tuneable antennas for brain implantable wireless medical microsystems, IEEE Trans. Antenn. Propag. 69 (2) (2020) 760–768.
[24] C.R. Liu, Y.X. Guo, S.Q. Xiao, Capacitively loaded circularly polarized implantable patch antenna for ISM band biomedical applications, IEEE Trans. Antenn. Propag. 62 (5) (2014) 2407–2417.
[25] J. Shang, Y. Yu, L.-J. Xu, Compact dual band implantable planar Inverted-F antenna with bandwidth enhancement, Microw. Opt. Technol. Lett. 62 (2020) 322–328.
[26] Vipan Kumar Gupta, Deepali Thakur, Design and performance analysis of a CPW-fed circularly polarized implantable antenna for 2.45 GHz ISM band, Microw. Opt. Technol. Lett. 62 (12) (2020) 3952–3959.
[27] Pournoori Nikta, Sydänheimo Lauri, Yahya Rahmat-Samii, Leena Ukkonen, Björninen Toni, Small triple-band meandered PIFA for brain-implantable biotelemetric systems: development and testing in a liquid phantom, Int. J. Antenn. Propag. 2021 (2021) 1–13.
[28] Moirangthem Santoshkumar Singh, Jeet Ghosh, Soumendu Ghosh, Abhishek Sarkhel, Miniaturized dual-antenna system for implantable biotelemetry application, IEEE Antenn. Wireless Propag. Lett. 20 (8) (2021) 1394–1398.
[29] D. Nikolayev, W. Joseph, A. Skrivervik, M. Zhadobov, L. Martens, R. Sauleau, Dielectric-loaded conformal microstrip antennas for versatile in-body applications, IEEE Antenn. Wireless Propag. Lett. 18 (12) (2019) 2686–2690.
[30] Geonyeong Shin, Yoon Ick-Jae, Investigation on insulated, brain-implanted antenna for highly reliable biotelemetry communication in MICS and ISM bands, Sensors 20 (1) (2019) 242.
[31] Geonyeong Shin, Wonkyo Kim, Min Cheol Kim, Jusung Kim, Jae-Young Chung, Junghyo Nah, Yoon Ick-Jae, A deionized water infilled dual-layer insulator applied brain-implanted UWB antenna for wireless biotelemetry applications, IEEE Trans. Antenn. Propag. (2022).
[32] Lisa Sapari, Samnang Hout, Jae-Young Chung, Brain implantable end-fire antenna with enhanced gain and bandwidth, Sensors 22 (12) (2022) 4328.
[33] Nikta Pournoori, Antenna Development in Brain-Implantable Biotelemetric Systems for Next-Generation of Human Healthcare, 2023.
[34] Leena Ukkonen, Lauri Sydänheimo, Toni Björninen, Stefanus Wirdatmadja, Nikta Pournoori, Merja Voutilainen, Antennas and wireless power transfer to small biomedical brain implants, in: 2022 IEEE MTT-S International Microwave Biomedical Conference (IMBioC), IEEE, 2022, pp. 239–241.
[35] G. Kumar, D. Singh, R. Kumar, A planar CPW fed UWB antenna with dual rectangular notch band characteristics incorporating U-slot, SRRs, and EBGs, Int. J. RF Microw. Computer-Aided Eng. 31 (7) (2021) e22676.
[36] Singh, Maninder, Dhawan Singh, Gurpreet Kumar, and Rajeev Kumar. "A Miniaturized and Circularly Polarized L-Shaped Slot Antenna for Ultra-wideband Applications.".
[37] B. Prudhvi Nadh, B.T.P. Madhav, M. Siva Kumar, M. Venkateswara Rao, T. Anilkumar, Circular ring structured ultra-wideband antenna for wearable applications, Int. J. RF Microw. Computer-Aided Eng. 29 (4) (2019) e21580.
[38] B.P. Nadh, B.T.P. Madhav, M.S. Kumar, Design and analysis of dual band implantable DGS antenna for medical applications, Sādhanā 44 (2019) 1–9.
[39] A. Iqbal, M. Al-Hasan, I.B. Mabrouk, M. Nedil, Scalp-implantable MIMO antenna for high-data-rate head implants, IEEE Antenn. Wireless Propag. Lett. 20 (12) (2021) 2529–2533.
[40] Andrzej Kraszewski, Prediction of the dielectric properties of two-phase mixtures, J. Microw. Power 12 (3) (1977) 216–222.
[41] H. Barakat, Julien Moussa, Ndagijimana Fabien, Study of effective permittivity for a multilayer substrate dipole antenna, International Journal of Microwave and Wireless Technologies 13 (9) (2021) 915–920.
[42] A. Gupta, A. Kansal, P. Chawla, Design of a patch antenna with square ring-shaped-coupled ground for on-/off body communication, Int. J. Electron. 106 (12) (2019) 1814–1828.